Supplementary Information

Dual Li-ion migration channels in ester-rich copolymer/ionic liquid quasi-solid-state electrolyte for high-performance Li-S batteries

Xiaomin Cai, Bei Ye, Jianlong Ding, Ziyun Chi, Liping Sun, Petr Saha, Gengchao Wang*

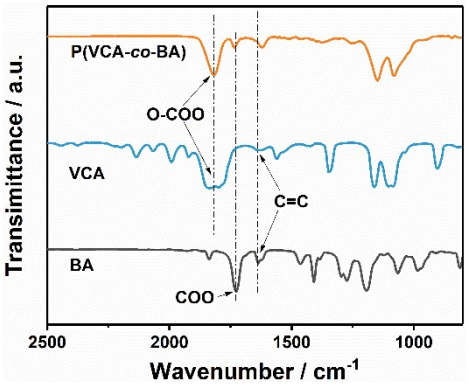

Fig. S1 FTIR spectra of BA, VCA, and P(VCA-*co*-BA).

It can be seen from the FTIR spectra Fig.S1 of the monomers and P(VCA-*co*-BA) that the VCA monomer has a strong absorption peak of carbonate group at 1833 cm^{-1}, C=C stretching vibration absorption at 1635 cm^{-1}, and C-O-C stretching vibration absorption peak connected by ester group at 1161 and 1102 cm^{-1}. At 1727 cm^{-1}, BA monomer was the strong absorption peak of ester based stretching vibration. At 1637 cm^{-1}, there was C=C stretching vibration absorption, and at 1274 and 1193 cm^{-1}, there was C-O-C stretching vibration absorption peak. The two strong absorption peaks of copolymer P(VCA-*co*-BA) at 1817 cm^{-1} and 1733 cm^{-1} correspond to the ester absorption peaks of VCA and BA respectively, and the C=C stretching vibration absorption peak disappears, which proves that the two monomers are successfully co-polymerized.

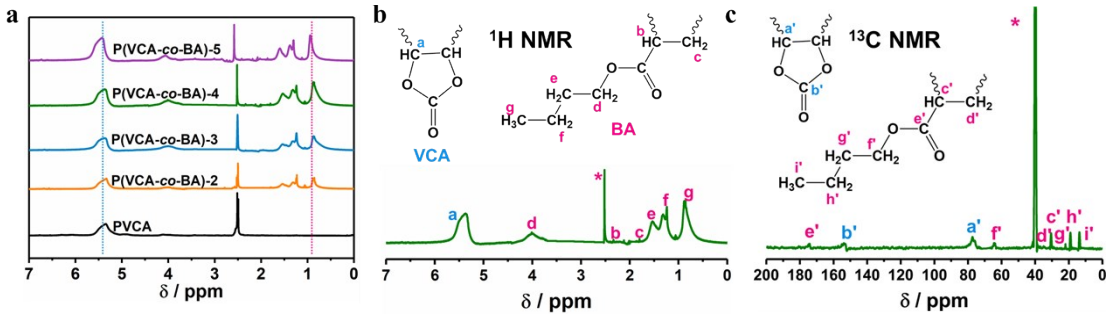

Fig. S2 (a) ^{1}H NMR spectra of PVCA and P(VCA-*co*-BA) copolymers with various VCA/BA feed ratios in DMSO-d_6, and (b) the corresponding details. (c) The ^{13}C NMR spectrum of P(VCA-*co*-BA)-4 in DMSO-d_6.

As shown in Fig.S3, the chemical structure of P (VCA-*co*-BA) was analyzed by ^{1}H NMR and ^{13}C NMR spectra. The proton chemical shift at 5.4 ppm represents the break of the -CH=CH- (8.0 ppm) in VCA (Fig.S3b), and the corresponding carbon chemical shift changes from 130 ppm of -CH=CH- to 77 ppm (Fig.S3c). In addition, 6.0-6.5 ppm (Fig.S3b) and 110-140 ppm (Fig.S3c) did not show the proton chemical shift and carbon chemical shift of the -CH=CH- in BA, which proved the breakage of the double bond in BA. It can be seen from Fig.S3a that the proton chemical shifts of PVCA at 5.4 ppm appears in the ^{1}H NMR spectra of P (VCA-*co*-BA)-2~5, and the unique absorption peaks of PBA at 0.86 ppm (-CH_3, g), 1.0-1.8 ppm (-CH_2-, c/e/f), and 4.0 ppm (-OCH_2, d), which proves that the two monomers have been successfully copolymerized. According to the integral area ratio of the characteristic absorption peaks of a and g, the composition ratio R_2^b of VCA/BA in the copolymer is calculated and listed in Table S1.

Table S1 Chemical composition and molecular weight of PVCA and P(VCA-*co*-BA) with various VCA/BA feed ratios

Samples	R_1[a]	R_2[b]	M_n (kDa)	M_w (kDa)	PDI
PVCA	1/0	1/0	160.9	191.1	1.19
P(VCA-*co*-BA)-5	5/1	3.0/1	220	330	1.50
P(VCA-*co*-BA)-4	4/1	2.8/1	243	384.1	1.58
P(VCA-*co*-BA)-3	3/1	2.5/1	175.7	399	2.27
P(VCA-*co*-BA)-2	2/1	1.6/1	229.4	472.5	2.06

[a] R_1 is feed molar ratio of VCA/BA.

[b] R_2 is VCA/BA molar ratio in copolymers from ^{1}H NMR analysis.

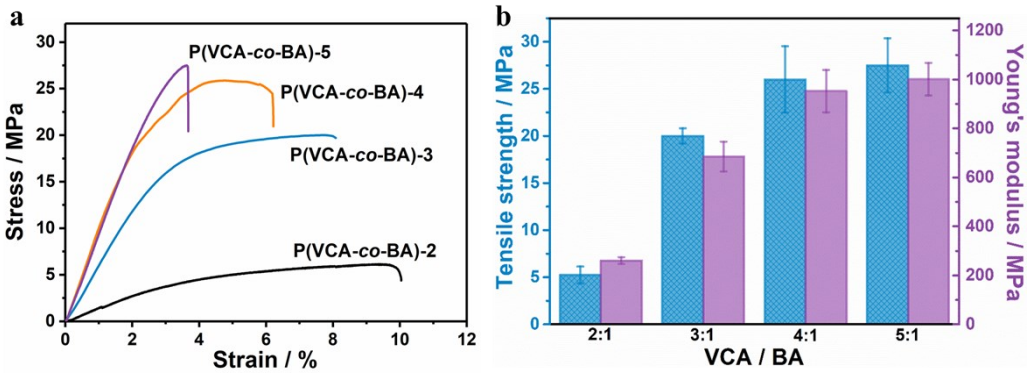

Fig. S3 (a) Stress-strain curves and (b) Tensile strength/Young's modulus of P(VCA-*co*-BA) with various VCA/BA feed ratios.

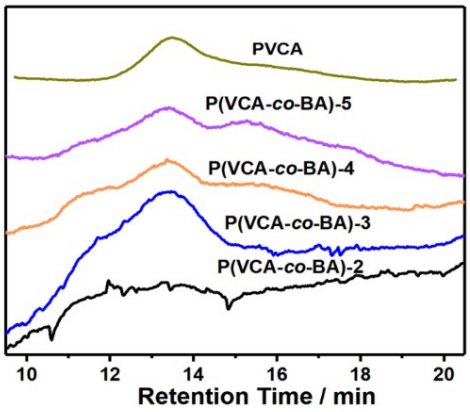

Fig. S4 Molecular weight distribution curves of PVCA and P(VCA-*co*-BA) copolymers with various VCA/BA feed ratios.

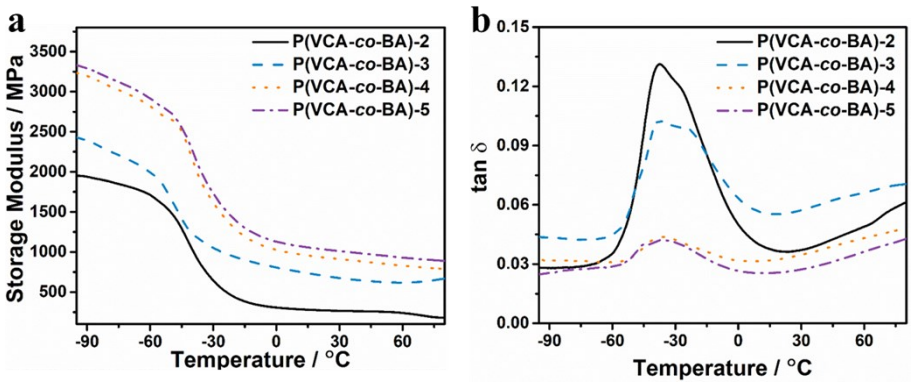

Fig. S5 (a) Storage modulus and (b) tan δ of P(VCA-*co*-BA) with various VCA/BA feed ratios.

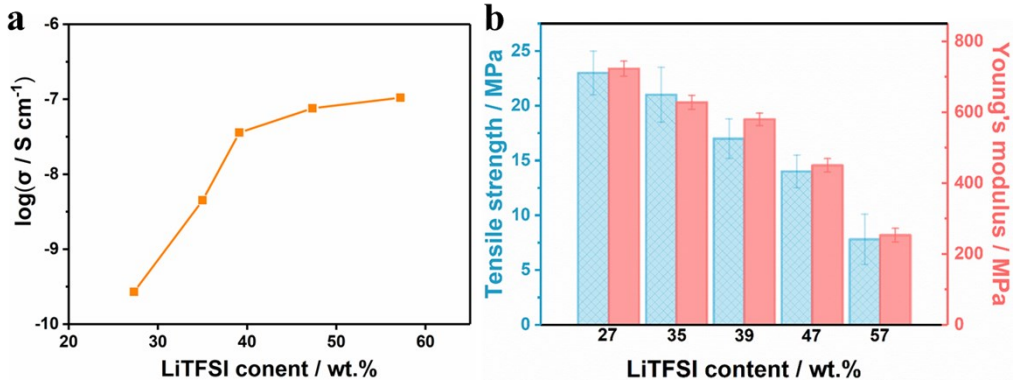

Fig. S6 (a) Ion conductivity and (b)Tensile strength / Young's modulus of P(VCA-*co*-BA)/LiTFSI solid electrolytes with different LiTFSI contents.

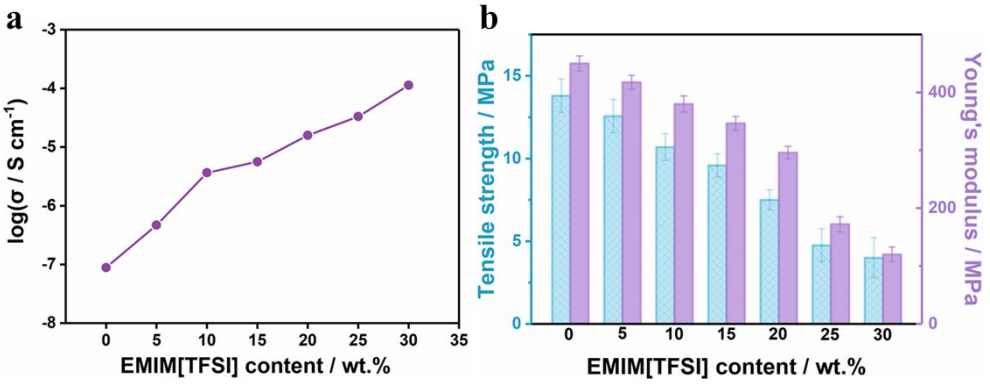

Fig. S7 (a) Ionic conductivity and (b) Tensile strength / Young's modulus of P(VCA-*co*-BA)/LiTFSI/[EMIM]TFSI with various EMIM[TFSI] contents.

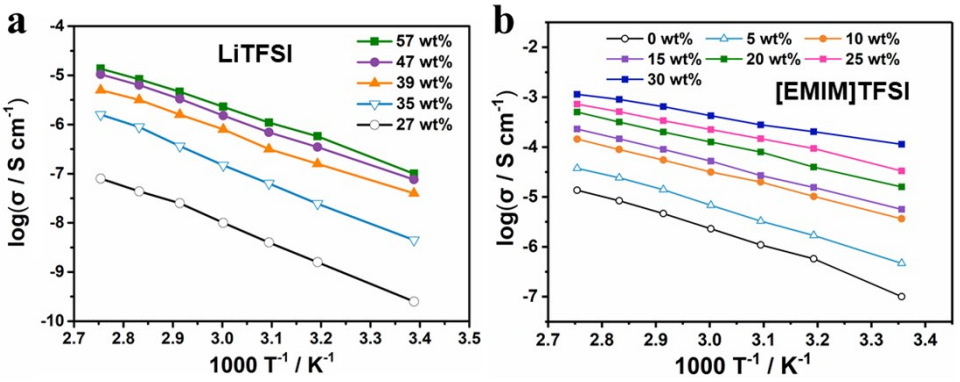

Fig. S8 Ion conductivity-temperature curves of P(VCA-*co*-BA)/LiTFSI solid electrolytes with different (a) LiTFSI and (b) [EMIM]TFSI contents.

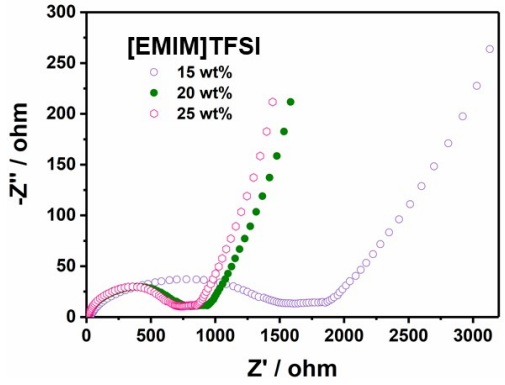

Fig. S9 Impedance spectra of Li//SPE-IL//Li cells with different [EMIM]TFSI contents at 25°C.

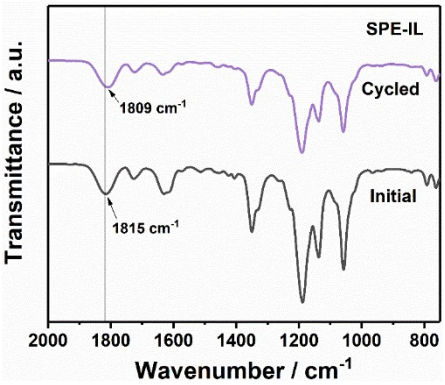

Fig. S10 FTIR spectra of SPE-IL before and after 300 cycles.

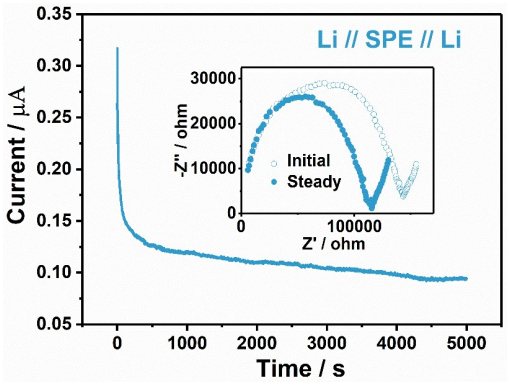

Fig. S11 Impedance spectra and DC polarization curve of Li//SPE//Li cell at 25°C.

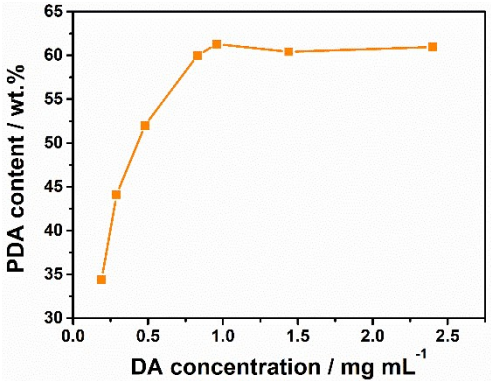

Fig. S12 Effect of dopamine concentration on PDA content of PDA-CNT films

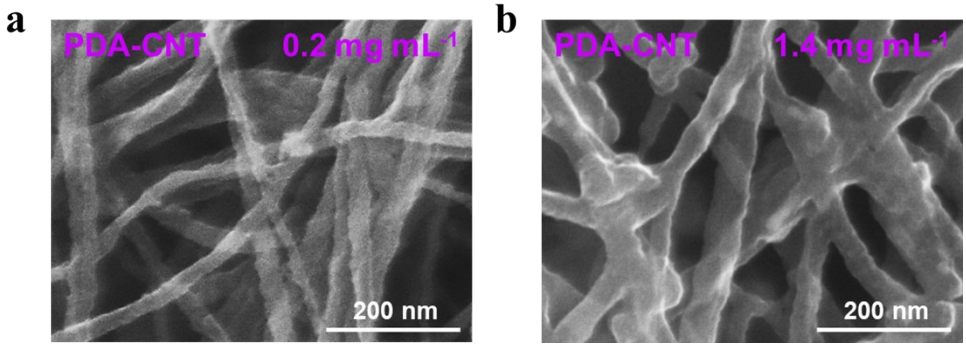

Fig. S13 FESEM images of PDA-CNT films prepared at dopamine concentrations of (a) 0.2 mg mL^{-1} and (b) 1.4 mg mL^{-1}.

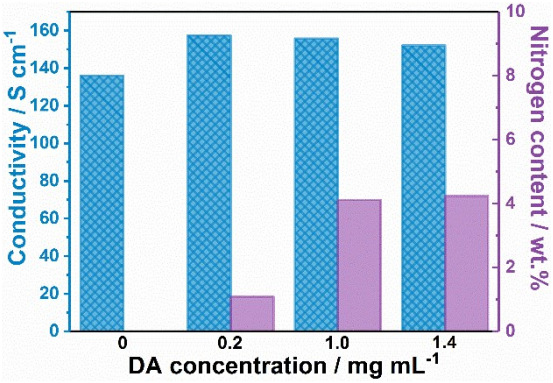

Fig. S14 Nitrogen content and electrical conductivity of N(PDA)-CNT films.

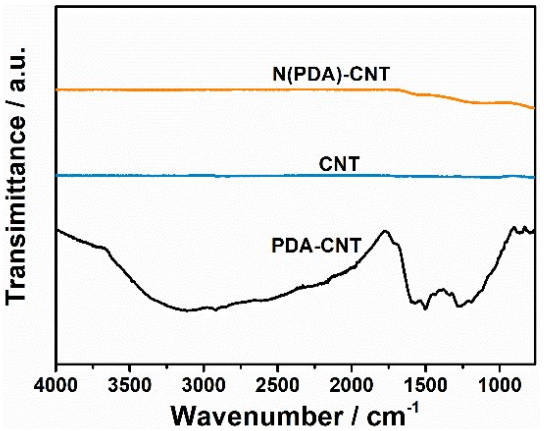

Fig. S15 ATR-FTIR spectra of CNT，PDA-CNT, and N(PDA)-CNT.

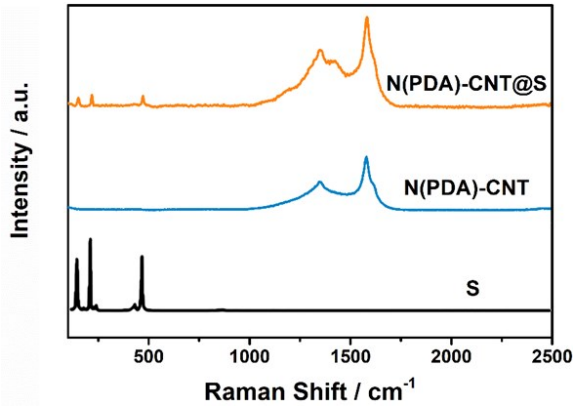

Fig. S16 Raman spectra of sulfur, N(PDA)-CNT film and N(PDA)-CNT@S composite film.

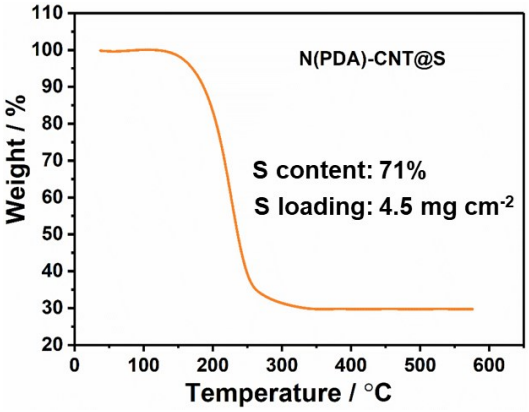

Fig. S17 TG curve of N(PDA)-CNT@S composite.

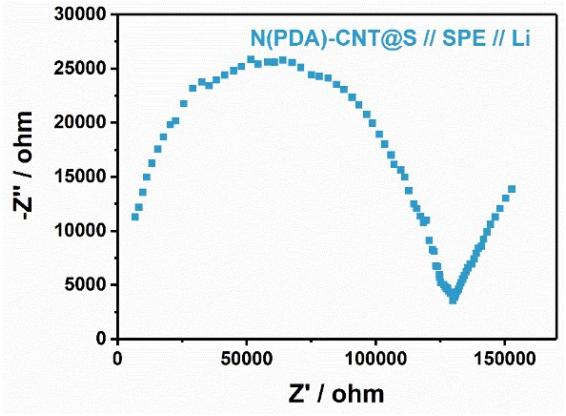

Fig. S18 Nyquist plots of N(PDA)CNT@S//SPE//Li battery at 25℃.

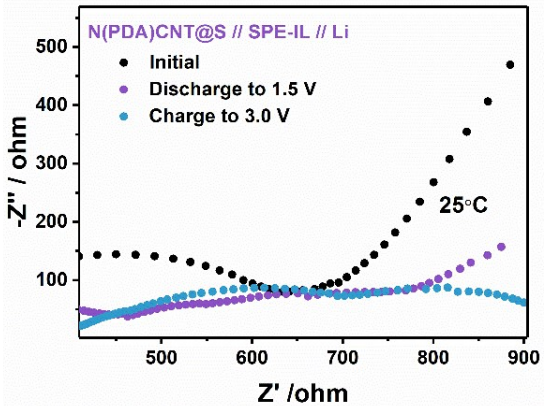

Fig. S19 Partial enlarged view of Fig. 4a.

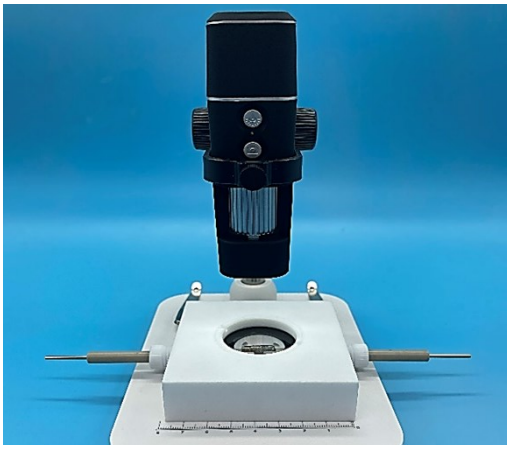

Fig. S20 Photos of in-situ electrolysis cell and high-power microscope lens.

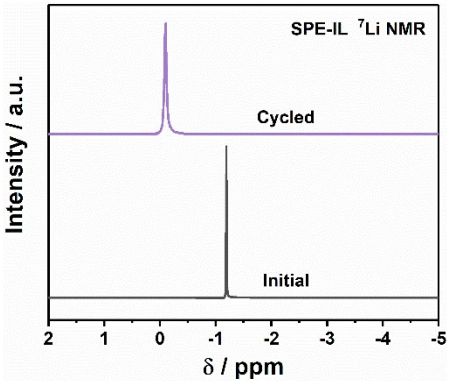

Fig. S21 ^{7}Li NMR spectra of SPE-IL before and after 300 cycles.

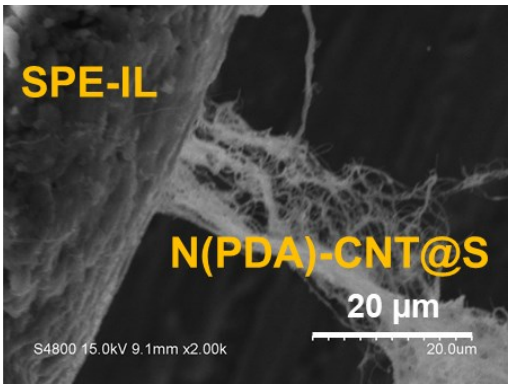

Fig. S22 Cross-section FE-SEM image of SPE-IL/N(PDA)CNT@S interface after 300 cycles.